J|A|C|S
ARTICLES

Published on Web 07/28/2009

Real-Time Electrochemical Monitoring of the Polymerase Chain Reaction by Mediated Redox Catalysis

Thibaut Defever,[†] Michel Druet,[†] Murielle Rochelet-Dequaire,[‡] Martine Joannes,[§] Céline Grossiord,[§] Benoit Limoges,*[,†] and Damien Marchal*[,†]

Laboratoire d'Electrochimie Moléculaire, Université Paris Diderot, UMR CNRS 7591, 15, rue Jean-Antoine de Baïf, 75205 Paris Cedex 13, France, Laboratoire des Interactions Muqueuses-Agents Transmissibles, Facultés de Médecine et de Pharmacie, EA 562, Université de Bourgogne, 7 Boulevard Jeanne d'Arc, 21000 Dijon, France, and Argene SA, Parc Technologique Delta Sud, 09340 Verniolle, France

Received February 22, 2009; E-mail: limoges@univ-paris-diderot.fr; marchal@univ-paris-diderot.fr

Abstract: We described the proof-of-principle of a nonoptical real-time PCR that uses cyclic voltammetry for indirectly monitoring the amplified DNA product generated in the PCR reaction solution after each PCR cycle. To enable indirect measurement of the amplicon produced throughout PCR, we monitor electrochemically the progressive consumption (i.e., the decrease of concentration) of free electroactive deoxynucleoside triphosphates (dNTPs) used for DNA synthesis. This is accomplished by exploiting the fast catalytic oxidation of native deoxyguanosine triphosphate (dGTP) or its unnatural analogue 7-deaza-dGTP by the one-electron redox catalysts $Ru(bpy)_3^{3+}$ (with bpy = 2,2′-bipyridine) or $Os(bpy)_3^{3+}$ generated at an electrode. To demonstrate the feasibility of the method, a disposable array of eight miniaturized self-contained electrochemical cells (working volume of 50 μL) has been developed and implemented in a classical programmable thermal cycler and then tested with the PCR amplification of two illustrated examples of real-world biological target DNA sequences (i.e., a relatively long 2300-bp sequence from the bacterial genome of multidrug-resistant *Achromobacter xylosoxidans* and a shorter 283-bp target from the human cytomegalovirus). Although the method works with both mediator/base couples, the catalytic peak current responses recorded with the $Ru(bpy)_3^{3+}$/dGTP couple under real-time PCR conditions are significantly affected by a continuous current drift and interference with the background solvent discharge, thus leading to poorly reproducible data. Much more reproducible and reliable results are finally obtained with the $Os(bpy)_3^{3+}$/7-deaza-dGTP, a result that is attributed to the much lower anodic potential at which the catalytic oxidation of 7-deaza-dGTP by $Os(bpy)_3^{3+}$ is detected. Under these conditions, an exponential decrease of the catalytic signal as a function of the number of PCR cycles is obtained, allowing definition of a cycle threshold value (C_t) that correlates inversely with the initial amount of target DNA. A semilogarithmic plot of C_t with the initial copy number of target DNA gives a standard linear curve similar to that obtained with fluorescent-based real-time PCR. Although the detection limit (10^3 molecules of target DNA in 50 μL) and sensitivity of the electrochemical method is not as high as conventional optical-based real-time PCR, the methodology described here offers many of the advantages of real-time PCR, such as a high dynamic range (over 8$-\log_{10}$) and speed, high amplification efficiency (close to 2), and the elimination of post-PCR processing. The method also has the advantage of being very simple, just requiring the use of low-cost single-use electrodes and the addition of a minute amount of redox catalyst into the PCR mixture. Moreover, compared to the other recently developed electrochemical real-time PCR based on solid-phase amplification, the present approach does not require electrode functionalization by a DNA probe. Finally, on account of the relative insensitivity of electrochemical methods to downscaling, the detection scheme is quite promising for use in miniaturized devices and in the development of point-of-care diagnosis applications.

Introduction

The introduction of real-time monitoring of the polymerase chain reaction (PCR) in the early 1990s was a major breakthrough in specific nucleic acid quantification.[1,2] The key feature of this technique is that the amplified DNA is quantified as it accumulates in the reaction, thereby eliminating laborious and time-consuming post-PCR analysis (e.g., end-point PCR assay on agarose gel or enzyme-linked oligonucleotidesorbent assay). So far, all of the real-time PCR methods are based on the optical detection of a fluorescent reporter molecule that produces an increase (or occasionally a decrease[3]) of fluorescence as the

[†] Université Paris Diderot.
[‡] Université de Bourgogne.
[§] Argene SA.

(1) Higuchi, R.; Dollinger, G.; Walsh, P. S.; Griffith, R. *Bio/Technology* **1992**, *10*, 413–417.
(2) Holland, P. M.; Abramson, R. D.; Watson, R.; Gelfand, D. H. *Proc. Natl. Acad. Sci. U.S.A.* **1992**, *88*, 7276–7280.
(3) Sherrill, C. B.; Marshall, D. J.; Moser, M. J.; Larsen, C. A.; Daudé-Snow, L.; Prudent, J. R. *J. Am. Chem. Soc.* **2004**, *126*, 4550–4556.

reaction proceeds.[4] These fluorescent reporter molecules include dyes that bind to the double-stranded DNA (e.g., SYBR Green),[5,6] or sequence-specific fluorescent oligonucleotide probes,[1,3,7−11] that fluoresce upon specific hybridization with the amplified DNA product. The resulting kinetic plot of fluorescence vs cycle number thus provides a way to monitor the PCR reaction in its early exponential phase, and it offers a route to quantitatively determine the initial number of DNA templates over a wide range of concentrations (more than 6 orders of magnitude).[4] This closed-tube analysis also has the benefit of reducing the risk of cross-contaminations.

On account of the inherent advantages of real-time PCR technology, namely, enhancements in accuracy, speed, and quantitation possibilities, it is rapidly becoming an indispensable tool in many fields of molecular diagnostics. Quantitative real-time PCR is, for example, commonly used for the determination of viral or bacterial loads,[12,13] identification and titers of germs in food,[14] diagnosis of tumors,[15] determination of single nucleotide polymorphisms,[16] and gene expression analysis.[17] Real-time PCR is also becoming increasingly important in forensic analyses.[18]

Regardless of their great success for analyzing nucleic acids, the existing fluorescence-based real time PCR instruments have some limitations. One limitation is the need for complex and delicate optical components that leads to rather fragile, bulky, and costly real-time PCR instruments, thereby restricting their use to clinical and research laboratories. Another shortcoming is the intercalating properties of fluorescent reagents that can partially inhibit the PCR reaction[19] whereas, in the case of fluorescent-labeled oligonucleotide probes, extensive efforts are required to optimize the protocol.[20] To overcome these limitations, an interesting prospect is to replace optical-based detection schemes with more robust, less expensive, and easier to miniaturize nonoptical sensing methods.

Most of the nonoptical approaches that have been developed for quantifying specific DNA sequences (some of them being founded on the intrinsic properties of DNA and others on the properties of an added indicator or label)[21−26] are based on the sequential hybridization of a single-stranded target sequence in solution to a complementary oligonucleotide capture probe immobilized on an electronic transducer surface, followed by end-point signal measurement of the hybridization events. Although these detection strategies are well-adapted to post-PCR analysis (i.e., after the completion of PCR), they are not easy to implement during PCR amplification. Even though some efforts have been made to integrate in the same miniaturized device a nonoptical detection of the enzyme amplification of nucleic acids, all were finally related to post-PCR detection.[27−32] To the best of our knowledge, the only example of a nonoptical method permitting measurement of DNA amplification during PCR is the one recently proposed by Hsing's group.[33,34] The principle is based on the coupling of a solid-phase PCR amplification (i.e., wherein the primers were directly attached and extended on the electrode surface) with the electrochemical detection of a surface-incorporated redox-labeled base. However, the major problem with this approach is the poor amplification efficiency of solid-phase polymerization that leads to a nonexponential growth of the signal. Such a problem is common with solid-phase PCR, and it is attributed to steric hindrance during solid-phase DNA hybridization and/or enzyme polymerization.[35−37] Another problem encountered by Hsing's group is an adverse effect of repetitive electrochemical scanning on the electrode response, which limits the real-time PCR measurement to a scarce number of cycles.[33] In view of these limitations, it is therefore highly desirable to develop an electrochemical

(4) Wilhelm, J.; Pingoud, A. *ChemBioChem* **2003**, *4*, 1120–1128.
(5) Higuchi, R.; Fockler, C.; Dollinger, G.; Watson, R. *Bio/Technology* **1993**, *11*, 1026–1030.
(6) Ririe, K. M.; Rasmussen, R. P.; Wittwer, C. T. *Anal. Biochem.* **1997**, *245*, 154–160.
(7) Tyagi, S.; Kramer, F. R. *Nat. Biotechnol.* **1996**, *14*, 303–308.
(8) Livak, K. J.; Flood, S. J.; Marmaro, J.; Giusti, W.; Deetz, K. *PCR Methods Appl.* **1995**, *4*, 357–362.
(9) Wittwer, C. T.; Herrmann, M. G.; Moss, A. A.; Rasmussen, R. P. *Biotechniques* **1997**, *22*, 130–138.
(10) Vet, J. A.; Majithia, A. R.; Marras, S. A.; Tyagi, S.; Dube, S.; Poiesz, B. J.; Kramer, F. R. *Proc. Natl. Acad. Sci. U.S.A.* **1999**, *96*, 6394–6399.
(11) Whitcombe, D.; Theaker, J.; Guy, S. P.; Brown, T.; Little, S. *Nat. Biotechnol.* **1999**, *17*, 804–807.
(12) Ratcliff, R. M.; Chang, G.; Kok, T.; Sloots, T. P. *Curr. Issues Mol. Biol.* **2007**, *9*, 87–102.
(13) Mackay, I. M.; Arden, K. E.; Nitsche, A. *Nucleic Acids Res.* **2002**, *30*, 1292–1305.
(14) Hernandez, M.; Rio, A.; Esteve, T.; Prat, S.; Pla, M. *J. Agric. Food Chem.* **2001**, *49*, 3622–3627.
(15) Bustin, S. A.; Gyselman, V. G.; Williams, N. S.; Dorudi, S. *Br. J. Cancer* **1999**, *79*, 1813–1820.
(16) Maas, F.; Schaap, N.; Kolen, S.; Zoetbrood, A.; Bruno, I.; Dolstra, H.; De Witte, T.; Schattenberg, A.; van De Wiel-van Kemenade, E. *Leukemia* **2003**, *17*, 621–629.
(17) Kubista, M.; Andrade, J. M.; Bengtsson, M.; Forootan, A.; Jonak, J.; Lind, K.; Sindelka, R.; Sjoeback, R.; Sjoegreen, B.; Stroembom, L.; Stahlberg, A.; Zoric, N. *Mol. Aspects Med.* **2006**, *27*, 95–125.
(18) Ye, J.; Parra, E. J.; Sosnoski, D. M.; Hiester, K.; Underhill, P. A.; Shriver, M. D. *J. Forensic Sci.* **2002**, *47*, 593–600.
(19) Monis, P. T.; Giglio, S.; Saint, C. P. *Anal. Biochem.* **2005**, *340*, 24–34.
(20) Boeckh, M.; Huang, M.; Ferrenberg, J.; Stevens-Ayers, T.; Stensland, L.; Nichols, W. G.; Corey, L. *J. Clin. Microbiol.* **2004**, *42*, 1142–1148.
(21) Drummond, T. G.; Hill, M. G.; Barton, J. K. *Nat. Biotechnol.* **2003**, *21*, 1192–1199.
(22) Fritz, J.; Baller, M. K.; Lang, H. P.; Rothuizen, H.; Vettiger, P.; Meyer, E.; Guntherodt, H.-J.; Gerber, C.; Gimzewski, J. K. *Science* **2000**, *288*, 316–318.
(23) Lee, H. J.; Wark, A. W.; Corn, R. M. *Langmuir* **2006**, *22*, 5241–5250.
(24) Xiao, Y.; Lubin, A. A.; Baker, B. R.; Plaxco, K. W.; Heeger, A. J. *Proc. Natl. Acad. Sci. U.S.A.* **2006**, *103*, 16677–16680.
(25) Patolsky, F.; Lichtenstein, A.; Willner, I. *Nat. Biotechnol.* **2001**, *19*, 253–257.
(26) Fritz, J.; Cooper, E. B.; Gaudet, S.; Sorger, P. K.; Manalis, S. R. *Proc. Natl. Acad. Sci. U.S.A.* **2002**, *99*, 14142–14146.
(27) Hou, C. S. J.; Milovic, N.; Godin, M.; Russo, P. R.; Chakrabarti, R.; Manalis, S. R. *Anal. Chem.* **2006**, *78*, 2526–2531.
(28) Hou, C. S. J.; Godin, M.; Payer, K.; Chakrabarti, R.; Manalis, S. R. *Lab Chip* **2007**, *7*, 347–354.
(29) Liu, R. H.; Yang, J.; Lenigk, R.; Bonanno, J.; Grodzinski, P. *Anal. Chem.* **2004**, *76*, 1824–1831.
(30) Gore, M. R.; Szalai, V. A.; Ropp, P. A.; Yang, I. V.; Silverman, J. S.; Thorp, H. H. *Anal. Chem.* **2003**, *75*, 6586–6592.
(31) Yeung, S. W.; Lee, T. M. H.; Cai, H.; Hsing, I.-M. *Nucleic Acids Res.* **2006**, *34*, e118.
(32) Lee, T. M. H.; Carles, M. C.; Hsing, I.-M. *Lab Chip* **2003**, *3*, 100–105.
(33) Yeung, S. S. W.; Lee, T. M. H.; Hsing, I.-M. *J. Am. Chem. Soc.* **2006**, *128*, 13374–13375.
(34) Yeung, S. S. W.; Lee, T. M. H.; Hsing, I.-M. *Anal. Chem.* **2008**, *80*, 363–368.
(35) Shapero, M. H.; Leuther, K. K.; Nguyen, A.; Scott, M.; Jones, K. W. *Genomes Res.* **2001**, *11*, 1926–1934.
(36) Pemov, A.; Modi, H.; Chandler, D. P.; Bavykin, S. *Nucleic Acids Res.* **2005**, *33*, e11.
(37) It is worth to note that the main drawback of solid-phase PCR is the dimer formation through molecular crowding and primer interference, which result in poor PCR amplification efficiency with an average value between 1.0 and 1.4,[36] whereas typical solution-phase amplification generally has an efficiency ranging from 1.6 to 2.0.

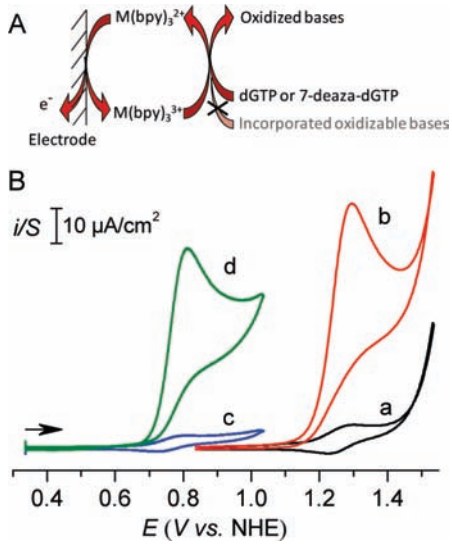

Figure 1. (A) Scheme principle of the selective redox catalytic oxidation of free oxidizable bases by electrogenerated $M(bpy)_3^{3+}$ (with M = Ru or Os). (B) CVs (v = 0.1 V s^{-1}) recorded in the electrochemical cell array maintained at 25 °C: (a) 20 μM $Ru(bpy)_3^{2+}$ alone; (b) 20 μM $Ru(bpy)_3^{2+}$ and 150 μM dGTP; (c) 10 μM $Os(bpy)_3^{2+}$ alone; (d) 10 μM $Os(bpy)_3^{2+}$ and 100 μM 7-deaza-dGTP. All solutions were prepared in a Tris-HCl buffer (50 mM, pH 8.7).

detection scheme that indirectly probes DNA polymerization in homogeneous solution phase instead of on the surface of an electrode.

Herein, we report the proof-of-principle of a nonoptical real-time PCR that uses cyclic voltammetry for indirectly monitoring the amplified DNA product generated in the reaction solution after each PCR cycle. To enable indirect measurement of the amplicon produced throughout PCR, we monitor electrochemically the progressive consumption of intrinsically electroactive deoxynucleoside triphosphates (dNTPs) used for DNA synthesis. This is accomplished by exploiting the fast catalytic oxidation of native deoxyguanosine triphosphate (dGTP) or its unnatural analogue 7-deaza-dGTP by the one-electron redox catalysts $Ru(bpy)_3^{3+}$ (with bpy = 2,2′-bipyridine) or $Os(bpy)_3^{3+}$ generated at an electrode (Figure 1A). Catalytic oxidation of intrinsically electroactive bases such as guanine, adenine, or some of their analogues by one-electron redox mediators such as $Ru(bpy)_3^{3+}$ has been widely investigated by Thorp's group to better understand electron-transfer reactions in DNA[38,39] and to develop new detection schemes for nucleic acids.[40−42] The main advantage of this detection strategy compared with direct oxidation of electroactive bases at an electrode is that it makes it possible to shift the oxidation wave to a potential (i.e., far from the potential discharge of the aqueous buffer) where well-defined and reproducible voltammetric current responses are obtained. These catalytic signals that are proportional to the concentration of catalyzed bases provide a basis for monitoring the concentration of free electroactive nucleobases during a PCR experiment, which should decrease exponentially with the number of PCR cycles, as the free dNTPs (i.e., unincorporated) are consumed to generate the amplified target DNA. For this statement to be true, it is necessary, of course, that the incorporated oxidizable dNTPs are less efficiently detected than their unincorporated counterpart. This should be true if, on the one hand, the bases incorporated into replicated DNA are less accessible to the catalyst for steric reasons and, on the other hand, under kinetic control of the catalytic current by mass transport, the diffusion coefficient of incorporated bases is significantly lower than the free base.

The validity of the method was examined for two illustrated examples of PCR amplification of real-world biological target DNA sequences. The first one was based on the PCR amplification of a relatively long DNA sequence (a 2300-bp coding for a class 1 integron gene cassette) from the bacterial genome of multidrug-resistant *Achromobacter xylosoxidans*, an aerobic Gram-negative bacillus that frequently colonizes the hospital environment and occasionally causes nosocomial infection.[43−45] The second one was derived from a commercial PCR kit for real-time monitoring of a 283-bp target from the human cytomegalovirus, a worldwide distributed virus that can provoke severe diseases in immunocompromised patients.[46]

Results and Discussion

To demonstrate the feasibility of this method, a disposable array of eight miniaturized self-contained electrochemical cells has been developed and implemented in a classical programmable thermal cycler. The hermetic seal of the eight electrochemical cells was obtained by pressure closing, between two clamped copper plates, a strip of eight polypropylene domed caps over a planar pattern array of 8 × 3 band-electrodes[47] screen-printed on a polyester substrate (Figure 2). Such an electrochemical cell configuration makes it possible to do cyclic voltammetry in a few tenths of a microliter of solution (in the present work, 50 μL) under programmed thermal cycles. Because of the significant thermal inertia conveyed by the copper plate holders, a maximal heating and cooling rate of ±1 °C/s was achieved.

Figure 1B compares the cyclic voltammograms (CVs) of the two selected mediator/base couples, i.e. $Ru(bpy)_3^{2+}$/dGTP and $Os(bpy)_3^{2+}$/7-deaza-dGTP, recorded in the electrochemical cell array at 25 °C. Each couple can be easily differentiated from the distinct potential at which the catalysis takes place. As expected from the standard potential of $Os(bpy)_3^{3+/2+}$ (E^0 = 0.76 V vs NHE), lower than that of $Ru(bpy)_3^{3+/2+}$ (E^0 = 1.26 V vs NHE), and from the easier oxidation of 7-deaza-dGTP than that of dGTP, the catalytic oxidation of 7-deaza-dGTP by the electrochemically generated $Os(bpy)_3^{3+}$ occurs at an anodic potential (∼0.8 V vs NHE) much lower than that of dGTP by $Ru(bpy)_3^{3+}$ (∼1.3 V vs NHE). Under the selected experimental conditions, well-defined, scan-rate-dependent, peak-shaped cata-

(38) Szalai, V. A.; Thorp, H. H. *J. Am. Chem. Soc.* **2000**, *122*, 4524–4525.
(39) Sistare, M. F.; Codden, S. J.; Heimlich, G.; Thorp, H. H. *J. Am. Chem. Soc.* **2000**, *122*, 4742–4749.
(40) Armistead, P. M.; Thorp, H. H. *Bioconjugate Chem.* **2002**, *13*, 172–176.
(41) Yang, I. V.; Ropp, P. A.; Thorp, H. H. *Anal. Chem.* **2002**, *74*, 347–354.
(42) Napier, M. E.; Loomis, C. R.; Sistare, M. F.; Kim, J.; Eckhardt, A. E.; Thorp, H. H. *Bioconjugate Chem.* **1997**, *8*, 906–913.
(43) Legrand, C.; Anaissie, E. *Clin. Infect. Dis.* **1992**, *14*, 479–484.
(44) Reverdy, M. E.; Freney, J.; Fleurette, J.; Coulet, M.; Surgot, M.; Marmet, D.; Ploton, C. *J. Clin. Microbiol.* **1984**, *19*, 140–143.
(45) Neuwirth, C.; Freby, C.; Ogier-Desserrey, A.; Perez-Martin, S.; Houzel, A.; Péchinot, A.; Duez, J.-M.; Huet, F.; Siebor, E. *Emerg. Infect. Dis.* **2006**, *12*, 1737–1739.
(46) Gouarin, S.; Vabret, A.; Scieux, C.; Agbalika, F.; Cherot, J.; Mengelle, C.; Deback, C.; Petitjean, J.; Dina, J.; Freymuth, F. *J. Virol. Methods* **2007**, *146*, 147–154.
(47) Disposable carbon-based screen-printed electrodes are particularly well adapted for the goal of the work because they can be easily mass produced at low cost with a high degree of flexibility in the pattern design. Moreover, they possess low background current and good reproducibility.

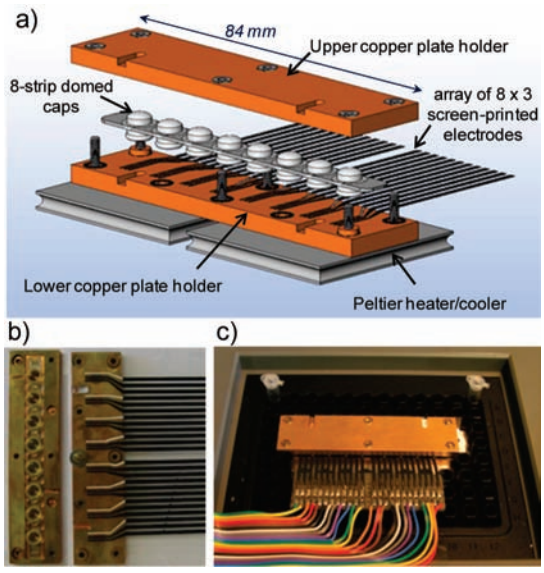

Figure 2. (a) Open view of the eight self-contained electrochemical cells. (b) Photography of the open electrochemical cells, showing on the left the cap containers ready to be fill with the mix of PCR, and on the right the array of 8 × 3 screen-printed electrodes including a reference Ag/AgCl electrode, a carbon working electrode, and a carbon counter electrode. (c) Overview of the sample holder when mounted in the thermocycler chamber and connected to the potentiostat.

lytic waves were observed for both couples. Such behavior is characteristic of efficient catalysis that leads to partial or total kinetic control of the catalytic response by mass transport of the oxidizable base.[48] These catalytic conditions were deliberately selected because, under a limiting case of total catalysis involving a nernstian redox mediator, the catalytic peak current ($i_{p,cat}$) should vary linearly with the concentration of base according to eq 1:[48]

$$i_{p,cat} = 0.609nFSC_B^0\sqrt{D_B}\sqrt{Fv/RT} \quad (1)$$

where n is the number of electron involved in the process, C_B^0 the base concentration, D_B its diffusion coefficient, S the electrode area, and v the scan rate. At a mediator concentration higher than 5 μM and a scan rate $\leq$0.3 V s^{-1}, a linear relationship between $i_{p,cat}$ and C_B^0 was effectively obtained within the base concentration range 0.2−200 μM for both mediator/base couples tested (not shown), with a detection limit of 0.1 μM.

An important prerequisite for the validity of the method is to have a highly stable and reproducible catalytic peak current under PCR cycling conditions. During our preliminary work with the $Ru(bpy)_3^{2+}$/dGTP couple, the catalytic current under simulated thermal cycles of PCR was strongly affected by the interference of the solvent/electrolyte discharge. The foot of the latter was indeed observed to continuously shift and grow in the direction of lower anodic potential until it interfered with the catalytic response (see Figure S1 in Supporting Information). This effect was attributed to the presence of chloride ions in the Tris-HCl buffer, the latter being more easily oxidized, as the working screen-printed carbon electrode was increasingly activated by thermal PCR cycling. To avoid this problem, the overall chloride anions contained in the standard PCR Tris-HCl buffer as well as in the $MgCl_2$ and KCl additives were systematically substituted by sulfate anions.[49] Figure 3 illustrates the stability of the catalytic response under simulated PCR conditions in Tris-H_2SO_4 buffer for the two mediator/base couples. The data were obtained from two distinct experiments in two separate arrays of electrochemical cells that were subjected to a series of typical three temperature step cycles (i.e., >94, 51−54 °C, and 72 °C) to simulate PCR, whereas the cyclic voltammetric responses were measured during the lowest temperature step. For both of the mediator/base couples, CVs (Figure 3A and 3B) as well as plots of the catalytic peak current with the number of thermal cycles (Figure 3C) exhibit a great stability and reproducibility (lower than 1.5%) throughout the overall thermal cycles. We have only noticed a small continuous increase and negative shift of the solvent discharge in the catalytic oxidation wave of dGTP by $Ru(bpy)_3^{3+}$ (indicated by the red arrow in Figure 3A) which reflects the occurrence of the solvent discharge interference even in Tris-H_2SO_4 buffer. Such an effect was not observed in the case of the $Os(bpy)_3^{2+}$/7-deaza-dGTP couple because catalysis takes place at a much lower anodic potential. The constant value of the catalytic peak current as a function of thermal cycles also reveals that the oxidizable base concentration remains constant throughout the experiment and that the cumulative amount of base irreversibly oxidized (i.e., consumed) upon repetitive voltammetric scans is negligible.[50]

The high stability of catalytic current has encouraged us to monitor electrochemically the PCR amplification of a target DNA sequence. Because the fraction of incorporated dNTPs not only depends on the number of target sequences generated but also on their size, we have first investigated the amplification of a relatively long DNA fragment in such a way to ensure a maximal catalytic current decrease during PCR reaction. The specific PCR amplification of the 2300-bp target sequence of resistant *A. xylosoxidans* was carried out using the same primers L1−R1 as previously described.[51] It was also directly performed on real biological samples (sputa of a cystic fibrosis patient infected with the bacteria) that were simply boiled and centrifugated before PCR amplification. To ensure high amplification efficiency and fidelity of the long target DNA, a blend of two thermostable DNA polymerase enzymes (mix of *Taq* plus a lesser amount of a proofreading *Tgo* DNA polymerase) was used.[52] A first attempt of real-time electrochemical PCR was then carried out on the basis of the electrocatalytic detection of dGTP by the electrochemically generated $Ru(bpy)_3^{3+}$. For such a purpose, the eight-strip electrochemical cell array was filled with a PCR mix containing (positive control) or not (negative control) the DNA template of resistant *A. xylosoxidans*. The overall solutions were then subjected to 30 PCR cycles, and the voltammetric catalytic current of each electrochemical cell

(48) Andrieux, C. P.; Savéant, J.-M. in *Electrochemical Reactions in Investigation of Rates and Mechanisms of Reactions; Techniques of Chemistry*; Bernasconi, C. F., Ed.; Wiley: New York, 1986; Vol. VI/4E, Part 2, pp305−390.

(49) The Tris-HCl buffer was replaced by a Tris-H_2SO_4 buffer (pH 8.7), and the $MgCl_2$ and KCl salts, required for optimal functioning of the enzyme polymerase, were substituted by $MgSO_4$ and NH_4SO_4 salts, respectively. The concentrations of these two latter additives were also optimized so as to have PCR yields as high as for standard Tris-HCl buffer.

(50) To avoid significant electrochemical consumption of the base throughout the repetitive cyclic voltammetric scans, the self-contained electrochemical cells were designed with a small electrode area/solution volume ratio of 0.4.

(51) Levesque, C.; Piche, L.; Larose, C.; Roy, P. H. *Antimicrob. Agents Chemother.* **1995**, *39*, 185–191.

(52) Barnes, W. M. *Proc. Natl. Acad. Sci. U.S.A.* **1994**, *91*, 2216–2220.

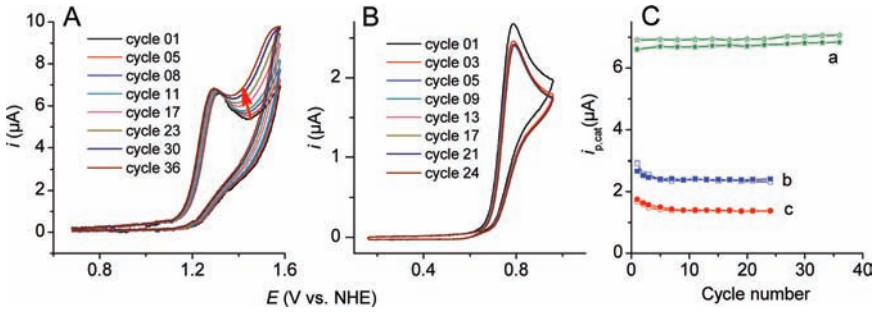

Figure 3. Series of CVs ($v = 0.3$ V s^{-1}) recorded in the electrochemical cell array under PCR cycling conditions. The cells were filled with (A) 50 μL of Tris-H_2SO_4 buffer (pH 8.7) containing 20 μM $Ru(bpy)_3^{2+}$ and 150 μM of each of the four dNTPs, (B) 50 μL Tris-H_2SO_4 buffer containing 10 μM $Os(bpy)_3^{2+}$, 100 μM 7-deaza-dGTP, 100 μM dGTP, and 200 μM each of dATP, dTTP, and dCTP. The thermal PCR cycling parameters were (A) 10 min at 95 °C, followed by 36 cycles of 60 s at 95 °C, 120 s at 51 °C, and 90 s at 72 °C; (B) 210 s at 94 °C, followed by 24 cycles of 90 s at 94 °C, 140 s at 54 °C, and 210 s at 72 °C. CVs were acquired once every two cycles at the end of the (A) 51 °C and (B) 54 °C heating phase (only a few cycles were overlaid as indicated in the legend). (C) Plots of $i_{p,cat}$ as a function of cycle number: (a) same conditions as in A; (b) same conditions as in B; (c) same as in B except for 50 μM 7-deaza-dGTP and 150 dGTP (each experiment was performed in duplicate).

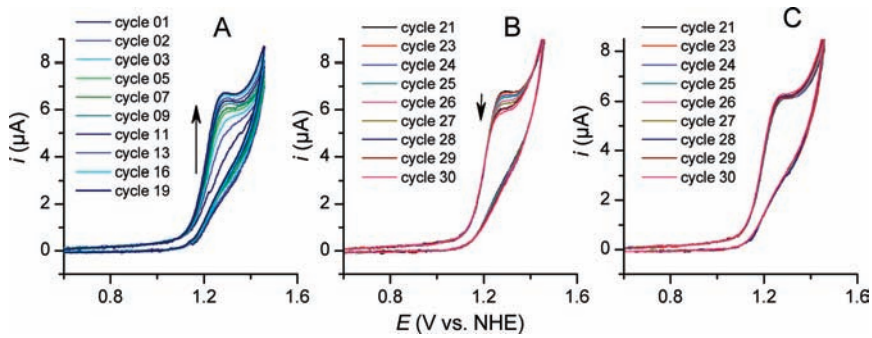

Figure 4. (A−C) Overlays of CVs ($v = 0.3$ V s^{-1}) showing progress of the electrocatalytic oxidation of dGTP (150 μM) by $Ru(bpy)_3^{3+}$ (20 μM) during PCR amplification of the 2300-bp target DNA of resistant *A. xylosoxidans*: (A, B) positive control, (C) negative control. The PCR cycle number is indicated in the legend.

was recorded during the annealing step of each PCR cycle.[53] Two typical series of CVs recorded at different numbers of cycles are shown in Figure 4. The first series was obtained from an electrochemical cell containing a positive DNA template (A and B) while the second one was from a negative control (C) (the CV curves recorded during the early PCR cycles for the negative control are not shown because they were very similar to those reported in A for the positive control). The catalytic currents at 1.3 V (vs NHE) were also reported as a function of the number of PCR cycles for all of the electrochemical cells tested (see Figure S2 in Supporting Information). Whatever the sample tested (i.e., negative or positive control), an unexpected systematic rapid increase of the catalytic response was observed during the early cycles, followed by a slower but continuous increase in the middle cycles. This unexpected drift of the catalytic response with PCR cycles was ascribed to the added DNA polymerase solution because in the absence of enzyme a horizontal baseline similar to those shown in Figure 3C was found.[54] Despite this considerable drift, a noticeable current decrease in the late cycles was clearly distinguished for the positive control (Figure 4B) but not for the negative one (Figure 4C) (this was systematically observed for all positive and negative controls tested; see Figure S2 of Supporting Information). To confirm that the signal decrease was indirectly related to the formation of amplified DNA product, the electrochemical cell contents were post-PCR-analyzed by gel electrophoresis and, as expected, a characteristic fluorescent band of the amplified 2300-bp target DNA was observed for all positive controls (see inset of Figure S2 in Supporting Information). The important drift of the catalytic response (several times larger than the decrease in current) combined with the occurrence of the solvent discharge interference was however detrimental to the reproducibility and robustness of the method. We have then anticipated that by lowering the catalytic detection far from the solvent discharge a more stable signal would be obtained. For this reason, we have examined the possibilities offered by the $Os(bpy)_3^{2+}$/7-deaza-dGTP couple. We have first verified the effect of the replacement of dGTP by 7-deaza analogue and the addition of $Os(bpy)_3^{2+}$ to the PCR reaction by examining the end-PCR product yield. For such a purpose, we have performed PCR amplifications of a resistant *A. xylosoxidans* template in standard PCR microtubes using different $Os(bpy)_3^{2+}$ concentrations and 7-deaza-dGTP/dGTP ratios. After 30 PCR cycles, the end-PCR products were analyzed by gel electrophoresis. The image of the gel (Figure 5) revealed no significant influence of $Os(bpy)_3^{2+}$ (in the range of 2.5−25 μM) on the final product yield of the PCR reaction because the intensity of the fluorescent band accredited to the 2300-bp amplicon was

(53) The programmed times for each temperature step of the cycle were made relatively long because of significant thermal inertia of the electrochemical cell. At 0.3 V s^{-1}, it takes less than 5 s to record one voltammogram, so the overall cells of the array could be entirely scanned during the annealing step of each cycle.

(54) Among the different additives present in the commercialized DNA polymerase solution, surfactants used to stabilize the enzyme were suspected to affect the catalytic response by adsorption on the electrode surface. Unfortunately, in the absence of precise knowledge of constituents contained in the supplied proprietary enzyme solution, it was not possible to clearly identify the additive responsible for this phenomenon.

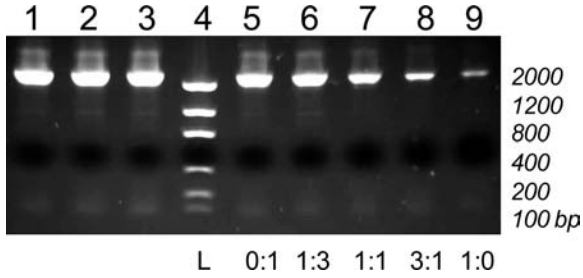

Figure 5. Gel electrophoresis image showing the influence of the $Os(bpy)_3^{2+}$ and 7-deaza-dGTP/dGTP ratios on the PCR amplification of resistant *A. xylosoxidans* DNA template. The PCR amplification was carried out in standard PCR microtubes in the presence of (lanes 1−3) 200 μM dNTP and different concentrations of $Os(bpy)_3^{2+}$ (i.e., 2.5, 10, 25 μM) and (lanes 5−9) in the absence of $Os(bpy)_3^{2+}$ but with different 7-deaza-dGTP/dGTP ratios (the ratios indicated on the figure were varied from 100% dGTP, lane 5, to 100% 7-deaza-dGTP, lane 9, keeping constant the total concentration of 7-deaza-dGTP and dGTP at a value of 200 μM). The overall microtubes were subjected to 30 PCR cycles (denaturation at 94 °C for 90 s, primer annealing at 54 °C for 140 s, and extension at 72 °C for 210 s) and the end-PCR product analyzed by gel electrophoresis. Lane 4: 100 bp DNA ladder.

the same as without added $Os(bpy)_3^{2+}$. This was not the case upon changing the 7-deaza-dGTP/dGTP ratios because a gradual decrease of the fluorescent band intensity was observed as the fraction of 7-deaza-dGTP was raised. This result is in agreement with earlier studies where it was shown possible to generate PCR products with complete replacement of native guanine by 7-deaza-guanine but to the detriment of end-PCR product yield that decreases upon increasing the 7-deaza-dGTP/dGTP ratio.[55,56] It is important to recall here that the intensity of the bands on the post-PCR gel electrophoresis (Figure 5) reflects the amount of amplicon produced at the end of the PCR (i.e., on the PCR plateau phase). This amount (which also corresponds to the end-PCR product yield) is dependent on factors (polymerase inactivation, primers consumption, etc.) that are not identical to those occurring in the exponential PCR amplification phase. Therefore, it is not possible on the basis of the post-PCR gel electrophoresis to make a conclusion on the incorporation efficiency of 7-deaza-dGTP relative to dGTP. Although it seems possible to carry out PCR with 100% 7-deaza-dGTP, for the further experiments we have finally preferred to work with a mixture of 7-deaza-dGTP/dGTP in such a way to favor PCR yield and thus the amplitude of signal decrease.

The electrochemical real-time PCR experiment previously performed with the first couple was then repeated with the $Os(bpy)_3^{2+}$/7-deaza-dGTP couple using different ratios of 7-deaza-dGTP/dGTP. An eight-strip electrochemical cell array was filled with two negative controls and six positive controls (containing the same input of resistant *A. xylosoxidans* DNA template) and then subjected to 37 PCR cycles. A typical series of voltammetric responses recorded for both a positive and negative control are shown in Figure 6A and 6B, respectively, and the raw and normalized catalytic peak currents as a function of cycle number for the complete eight cells are gathered in Figure 6C and 6D. In contrast to the preceding results obtained with the $Ru(bpy)_3^{2+}$/dGTP couple, much more stable baselines with only small linear drifts were consistently obtained. The linear baseline drifts were then easily corrected and normalized (see Materials and Methods). The normalized catalytic responses

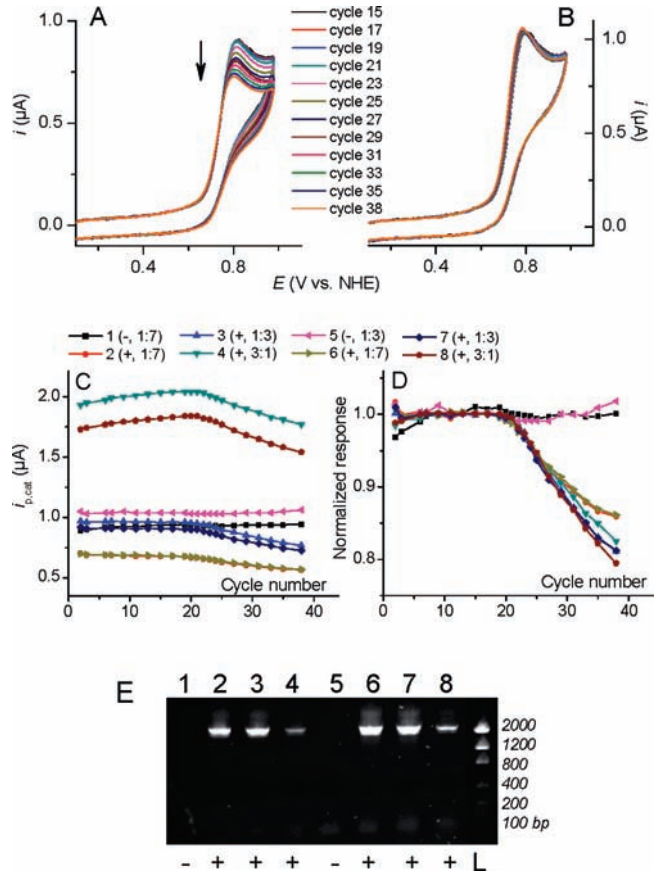

Figure 6. (A, B) Overlays of CVs (υ = 0.3 V s^{-1}) showing progress of the electrocatalytic oxidation of 7-deaza-dGTP (50 μM) by $Os(bpy)_3^{3+}$ (10 μM) during PCR amplification of a 2300-bp target DNA of resistant *A. xylosoxidans*: (A) positive control, (B) negative control. (C) Electrochemical-based real-time PCR curves obtained in the absence or presence of DNA template and for different ratios of 7-deaza-dGTP/dGTP. In the legend is mentioned the cell number in the array and, in parentheses, the positive or negative character of the PCR solution as well as the ratio value of 7-deaza-dGTP/dGTP. (D) Same as in C but after baseline correction and normalization. (E) Gel electrophoresis image of the electrochemical cell contents after PCR amplification (Lane L, 100 bp DNA ladder; lanes +, positive controls; lanes −, negative controls; numerals, cell number in the array).

show a systematic decrease for all positive controls and no change for negative controls. The decrease and absence of signal decrease were all correlated to the presence or absence of a 2300-bp fluorescent band on the post-PCR image of gel electrophoresis. The most striking feature of the normalized plots is the perfect overlay at which the signal starts to decrease (the average normalized signal at the 23 cycle was 0.971 ± 0.003, indicating a relative standard deviation of 0.3%), showing a much higher reproducibility with $Os(bpy)_3^{2+}$/7-deaza-dGTP detection scheme than with $Ru(bpy)_3^{2+}$/dGTP. The percentage of signal decrease (i.e., 15−20%) is similar to the one previously measured with the $Ru(bpy)_3^{2+}$/dGTP couple, and it does not change significantly with other 7-deaza-dGTP/dGTP ratios.

The next objective was to precisely evaluate the analytical performances of the proposed electrochemical-based real-time PCR compared with those of conventional fluorescent methods. However, in the absence of an accessible fluorescent-based real-time PCR for the 2300-bp sequence of resistant *A. xylosoxidans*, we decided to use an alternative target DNA for which a standardized fluorescent-based real-time PCR was commercially available, a 283-bp DNA sequence from the human cytomegalovirus (hCMV).[46] With the aim to determine the dynamic

(55) Seela, F.; Röling, A. *Nucleic Acids Res.* **1992**, *20*, 55–61.
(56) McConlogue, L.; Brow, M. A. D.; Innis, M. A. *Nucleic Acids Res.* **1988**, *16*, 9869.

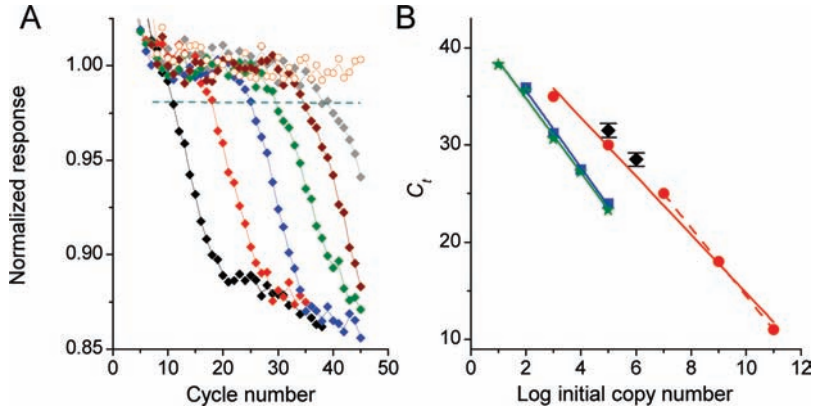

Figure 7. (A) Electrochemical-based real-time PCR curves for a 100-fold dilution series of 283-bp hCMV target DNA (from left to right: 10^{11}, 10^9, 10^7, 10^5, 10^3, 0 initial copies of target and negative control with one of the two primers omitted). The horizontal dashed line indicates the threshold level used to establish the C_t values. (B) Standard calibration plots of C_t vs the logarithmic input of hCMV copies for (■, ★) conventional fluorescence-based real-time PCR (TaqMan probes in a Rotor-Gene instrument) and (●, ◆) electrochemical-based real-time PCR. The data were obtained from serial dilutions of (■, ★, ◆) the same quantified biological extract of hCMV DNA template (2×10^5 copies/μL), or (●) a calibrated solution of 283-bp hCMV DNA amplicon (2.6×10^{10} copies/μL). Straight lines are linear regressions.

range of the method, kinetic PCR curves (Figure 7A) based on the electrocatalytic oxidation of 7-deaza-dGTP by $Os(bpy)_3^{3+}$ were at first generated from serial dilutions of a calibrated hCMV DNA amplicon (2.6×10^{10} copies/μL hCMV DNA) (see Materials and Methods). In this case, a HotStartTaq polymerase was used and the PCR mixes were prepared with a commercialized buffer (Qiagen PCR buffer).[57] As expected, the kinetic PCR curves show that the lower the starting amount of target DNA, and the higher the cycle number at which the normalized signal start to decrease. A signal decrease beyond the 40th PCR cycle was also obtained for the negative control. This behavior was attributed to unspecific amplification of primer-dimers or possibly other nonspecific PCR products because in the absence of one of the two primers the signal has remained unchanged all along the PCR cycles (open circle symbols in Figure 7A).[58] The noteworthy generation of nonspecific product obtained during this experiment is promoted by the slow heating and cooling rates of the actual electrochemical cell array because under the optimal conditions recommended by the manufacturer of the commercialized real-time PCR kit of the 283-bp hCMV DNA sequence (i.e., two-step temperatures with a shorter programmed cycle) we have not observed a significant primer-dimers band in post-PCR gel electrophoresis. An optimized cell, specially designed for fast heat transfer, should certainly lower the generation of unspecific product and also improve the PCR performance. For an optical real-time PCR system, the initial template concentration correlates inversely with the number of cycles required to increase the signal above a threshold level. Because we have the exact opposite (i.e., a signal decrease), the signal can then be analyzed based upon the number of cycles required to decrease the signal below a threshold value. This was accomplished by setting a threshold line across the graph as indicated in Figure 7A, from which the cycle threshold value (C_t) of each curve was defined as the intercept with this line. A plot of C_t vs $\log_{10}$ initial copy number of hCMV DNA (Figure 7B) gives a standard curve similar to that of fluorescent-based real-time PCR methodologies. The standard curve is linear over 8$-\log_{10}$ range with a correlation of 0.989 and a detection limit as few as 10^3 molecules of initial target DNA in the 50 μL PCR solution.

The C_t value is proportional to the logarithm of the initial amount of DNA template according to the linear eq 2.[4]

$$C_t = -\log(\varepsilon)^{-1} \log N_0 + b \qquad (2)$$

where ε is the amplification efficiency ($1 \leq \varepsilon \leq 2$), N_0 is the initial copy number of target DNA, and b is a constant that include a proportionality factor to relate PCR product concentration and signal intensity. From the slope of the linear regression of C_t vs $\log_{10} N_0$ we calculate an amplification efficiency of 2.12, which is higher than the maximal theoretical value of 2. This anomalously high ε value is explained by an increasing contribution of unspecific products as the starting concentration of target DNA is decreased. A better estimate of the amplification efficiency, free of nonspecific contributions, can then be found from linear regression to the highest concentrations (dashed line in Figure 7B). Under this condition, an amplification efficiency of 1.93 was calculated. Such a value close to 2 clearly shows that the unnatural 7-deaza-dGTP base does not affect the PCR amplification efficiency probably because it is incorporated as efficiently as the natural base.[55]

To evaluate the analytical performances of the proposed method and to compare with those of conventional fluorescent methods, the C_t values of serial dilutions of the same quantified biological extract of hCMV DNA template (2×10^5 copies/μL) were determined using both the electrochemical real-time PCR method and a conventional real-time PCR (using TaqMan fluorescent probes) on a Rotor-Gene system. The resultant data were used to plot the standard curves shown in Figure 7B. In the case of the fluorescent-based real-time PCR, the standard curve was determined using a standard PCR protocol but also according to our specific PCR conditions (i.e., in the presence of 10 μM $Os(bpy)_3^{2+}$ and 1:1 7-deaza-dGTP/dGTP ratio). From the slopes of the fluorescent calibration plots, PCR efficiencies of 1.83 and 1.79 were obtained, respectively, demonstrating that the presence of osmium complex and 7-deaza-dGTP do not significantly affect the PCR efficiency. However, comparison of the electrochemical C_t values with those of fluorescence shows a somewhat lower sensitivity of the electrochemical strategy (the shift of sensitivity is equivalent to about six PCR cycles). Because the sensitivity in real-time PCR is mainly

(57) The use of a commercial buffer was rendered possible because at the low anodic potential at which the catalytic oxidation takes place, there was no significant interference of chlorides ions brought by the buffer.
(58) We have obtained a similar result with a positive sample in which we have voluntary not added the polymerase into the PCR mixture.

related to the ability of detecting directly or indirectly a low amount of amplified DNA, it was interesting to evaluate such a parameter with the present method. A simple calculation gives an estimate that a 2% signal decrease on the electrochemical real-time PCR curve should correspond to a consumption of ca. 1 μM of free electroactive base over the 50 μM initially present in the PCR solution. Considering that the synthesis of each double strand of 283-bp hCMV DNA target requires the incorporation of 70 equiv of 7-deaza-dGTP (assuming equal incorporation efficiency of 7-deaza-dGTP and dGTP), the signal decrease of 2% should thus represent the indirect detection of ~15 nM of amplified target DNA.

Conclusion

Although the sensitivity is not as high as conventional optical-based real-time PCR, the methodology described here offers many of the advantages of real-time PCR, such as a high dynamic range of detection with quantitative potentialities and the elimination of post-PCR processing. The method also has the specific advantage of simplicity because it only requires the addition of a minute amount of redox catalyst into the PCR mixture, and even though the approach does not offer the additional specificity afforded by labeled hybridization probes, it simplifies the design issues and allows for rapid development. Moreover, compared to fluorescent approaches based on intercalating dyes such as SYBR Green, the electrochemical detection is not prone to inhibition artifacts, and the redox catalysts $Ru(bpy)_3^{2+}$ and $Os(bpy)_3^{2+}$ are much more stable than fluorescent probes, which is an advantage for handling and storage. The detection scheme was also demonstrated to be feasible with a relatively long DNA fragment. This is clearly a benefit compared to the existing fluorescent methods based on labeled hybridization probes which generally failed to monitor real-time PCR of long DNA sequences. The proposed method can finally be viewed as a complementary approach to existing methods, well adapted to measure an optimized standard PCR reaction.

An additional significance of the work is that it demonstrates the viability of electrochemically monitoring in real-time (i.e., at every PCR cycle) the exponential amplification of a homogeneous PCR reaction using a low-cost disposable multiplexed array of electrochemical cells (an important prerequisite for the manufacturing development of an economically viable instrument). Under these conditions, it was possible to plot, for the first time, a fully resolved kinetic PCR curve using a nonoptical method. This is a substantial improvement over the previous electrochemical solid-phase real-time PCR that was based on the use of rather cost-effective DNA probe-modified ITO electrodes, itself restricted to only one electrochemical measurement per electrode because of problems of memory effects and/or stability of the DNA-functionalized electrodes during the PCR experiment.[34] We expect that such a significant advance should open new opportunities to further development of electrochemical-based real-time PCR.

Further effort is now required to improve the practicality of the method and its analytical performance. Significant progress can be expected from the development of an entirely automated device with an improved cell design for faster thermal heat transfer. The detection scheme can also be simplified by attaching the redox catalyst to the electrode surface, a strategy that should improve both the selectivity and sensitivity of the catalytic detection and also eliminate the presence of catalyst in the final PCR product. Another important advancement can also be obtained through integration of the detection scheme in a miniaturized system, such as a microchip platform[34] or a microfluidic device.[32] This is supported by the fact that, in contrast to optical methods, the analytical performances of the electrochemical methods are relatively insensitive to downscaling. At the same time, the method would benefit from many improvements brought by miniaturization of PCR, including faster thermal response rate, reduced reagent consumption, and higher sample handling, without the drawbacks associated with fluorescent optical systems. Work is in progress aimed at achieving these goals.

Material and Methods

Reagents. The $Os^{II}(bpy)_3(PF_6)_2$ was synthesized as previously described,[59] and $Ru^{II}(bpy)_3Cl_2 \cdot 6H_2O$ (Aldrich) and 7-deaza-dGTP (TriLink Biotechnology) were used without further purification.

The positive biological sample containing the DNA template of resistant *A. xylosoxidans* was obtained from the sputa of a cystic fibrosis patient. Before PCR amplification, the genomic DNA was simply extracted from the cells by boiling the biological sample at 100 °C, and the residual fragments of cells in the supernatant were eliminated by centrifugation. The positive biological sample was kindly provided by the Département de Bactériologie of the Hospital of Dijon (France).

The quantified biological extract of hCMV DNA template (2×10^5 copies/μL) was obtained from a MRC5 cell line extract infected by AD169 CMV stain. The hCMV DNA extraction was realized with QIAamp DNA Blood Mini kit (Qiagen). The concentrated amplicon of 283-bp hCMV DNA (2.6×10^{10} copies/μL) was obtained from standard PCR amplification of the biological extract of hCMV DNA template. The copy number of hCMV target sequences contained in the concentrated amplicon was calibrated by gel electrophoresis.

PCR products were electrophoresed on a 2% agarose gel and were visualized by ethidium bromide staining.

Sample Holder. The sample holder shown in Figure 2 has been design around a disposable array of eight independent electrochemical cells. The eight self-contained electrochemical cells were assembled from eight-strip polypropylene-domed caps (ABgene) sealed over an array of 8×3 band-electrodes (a carbon working electrode, a carbon counter electrode, and a Ag/AgCl reference electrode) screen-printed on a flexible planar polyethylenterephtalate film. For a tight seal of the strip caps over the planar polyester substrate, the eight electrochemical cells were sandwiched between two copper plate holders clamped with six screws. Such an assembly defined for each cell a working electrode area of 0.02 cm^2, the latter being delimited by the inside diameter of the polyethylene cap apertures, and a working cell volume of 75 μL allowing the PCR to be performed in a reaction volume of 25−75 μL. The backside of the copper holder was mounted inside the chamber of a thermocycler (Swift Maxi thermal cycler from Esco).

A slight cell-to-cell variability in the magnitude of catalytic current was sometimes observed. This was caused by small cell-to-cell fluctuation of the working electrode areas, depending on the pressure used to seal the strip caps over the planar substrate of screen-printed electrodes. These electrode area fluctuations are not a problem because the electrode area remains constant within the same cell throughout the overall PCR experiment and also because the goal is to measure the percentage decrease of catalytic current.

Real-Time PCR Conditions for the *A. xylosoxidans*. Forward primer L1, 5′-GGCATCCAAGCAGCAAGC-3′, and reverse primer R1, 5′-AAGCAGACTTGACCTGAT-3′, were used to amplify a 2300-bp fragment of resistant *A. xylosoxidans*, specific for a class 1 integron gene cassette.[51] The PCR buffer consisted of 50 mM Tris-H_2SO_4 buffer (pH 8.7), 1.5 mM $MgSO_4$, and 3 mM NH_4SO_4.

(59) Kober, E. M.; Caspar, J. V.; Sullivan, B. P.; Meyer, T. J. *Inorg. Chem.* **1988**, *27*, 4587–4598.

In the case of catalytic oxidation of dGTP by $Ru(bpy)_3^{3+}$, the PCR reaction mixture (50 μL) included the PCR buffer, 20 μM $Ru(bpy)_3(PF_6)_2$, 0.15 mM each of dNTPs, 0.5 μM each of forward and reverse primers, 0.75 units of polymerase blend from the Expand High Fidelity PCR system (Roche Diagnostics), and positive control templates (2.5 μL). For the negative control, the DNA template suspension was replaced by water. PCR cycling conditions were as follows: initial denaturation at 94 °C for 210 s, followed by 30 cycles of 94 °C for 90 s, 140 s annealing at 54 °C, and 210 s extension at 72 °C. After the 10th cycle, the extension step was iteratively incremented for 5 s (the increment of the extension step duration is important for improving the amplification of long DNA fragment). The cyclic voltammograms were recorded ($v = 0.3$ V s^{-1}) during the annealing step at 54 °C and for each cycle.

In the case of catalytic oxidation of 7-deaza-dGTP by $Os(bpy)_3^{3+}$, the PCR reaction mixture (50 μL) was composed of 10 μM $Os(bpy)_3(PF_6)_2$, 0.2 mM each of dATP, dCTP, and dTTP, $(0.2 - x)$ mM dGTP, x mM 7-deaza-dGTP (with $x = 0.025$, 0.05, or 0.15 mM), 0.5 μM each of forward and reverse primers, 0.75 units of polymerase blend from the Expand High Fidelity PCR system kit (Roche Diagnostics), 2.5 μL of positive control templates, and the PCR buffer. PCR cycling conditions were exactly the same as those used the preceding case, except that instead of using 20 supplementary cycles, 27 were applied. The cyclic voltammograms were again recorded ($v = 0.3$ V s^{-1}) during the annealing step at 54 °C and for each cycle.

Baseline correction of the kinetic PCR curves was achieved by subtracting a least-squares fitted line across 10 cycles immediately before signal decreases. Current normalization was next accomplished by offsetting the data sets to align the value of the 11th PCR cycle.

Real-Time PCR Conditions for the hCMV DNA. Specific primers, provided by Argene (proprietary sequences), were used to amplify a 283-bp hCMV DNA fragment targeting UL83 gene coding for phosphoprotein pp65.[46] The PCR reaction was performed in Qiagen buffer 1X (50 μL) containing 10 μM $Os(bpy)_3(PF_6)_2$, 0.2 mM each of dATP, dCTP, and dTTP, 0.15 mM dGTP, 0.05 mM 7-deaza-dGTP, 0.2 μM each of forward and reverse primers, 1 unit of HotStartTaq polymerase (Qiagen), and 2.5 μL of serial dilution of the calibrated 283-bp hCMV DNA amplicon (2.6×10^{10} copies/μL) or 5 or 0.5 μL of the quantified biological extract of hCMV DNA (2×10^5 copies/μL). The PCR was performed according to the following thermal cycling: preheating period of 15 min at 92 °C followed by 45 cycles of 95 °C for 60 s, 53 °C for 120 s, and 72 °C for 120 s. The cyclic voltammograms were recorded at 53 °C during the annealing step of each PCR cycle.

The conventional fluorescent-based method (TaqMan PCR) was performed on a Rotor-Gene (Corbett Life Science). The PCR reaction was performed in 25 μL containing Qiagen buffer 1X, 0.2 mM of each dNTP, 0.5 μM of specific primers, 0.1 μM of specific probe (primers and probe provided by Argene), 1.875 units/PCR of HotStartTaq polymerase (Qiagen), and 10 μL of standard diluted solutions of the quantified biological extract of hCMV DNA template (final quantity ranging from 10 to 10^5 copies per assay). The PCR was performed at 95 °C for 15 min, followed by 45 cycles at 95 °C for 10 s, 60 °C for 40 s. The acquired fluorescence was measured during the step at 60 °C. For mimicking the electrochemical PCR conditions, the PCR reaction was performed similarly to standard conditions, except that 0.1 mM each of dATP, dCTP, and dTTP, 0.05 mM of dGTP, 0.05 mM 7-deaza-dGTP, and 10 μM $Os(bpy)_3(PF_6)_2$ were added to the PCR solution.

Electrochemical Measurements. Cyclic voltammetry was carried out with a PST20 Autolab potentiostat (Eco-Chemie) interfaced to a PC computer and connected to the electrochemical cell array through a homemade connector equipped with an eight-position selector switch. During our preliminary work, the voltammetric measurements at each cycle of PCR were started manually. We also later succeeded in the development of a homemade eight-channel multiplexed potentiostat entirely synchronized to the thermal cycles of the PCR. With such equipment it was possible to scan by cyclic voltammetry the eight electrochemical cells quasisimultaneously at the end of each annealing step of PCR cycle.

The screen-printed electrodes were prepared from a semiautomatic screen-printer (Presco, USA), using carbon (PF 407A) and silver (418SS) carbon inks (Acheson Colloid). For homogeneity and clarity, all potentials in the text were quoted relative to a normal hydrogen electrode (NHE).

Acknowledgment. This research was supported by Université Paris Diderot, CNRS, Region Bourgogne (partial Ph.D. financial support of T.D.) and Agence Nationale de la Recherche (ANR - EMPB - DETSCAN project). The authors thank Prof. R. Blankespoor for helpful corrections and editing.

Supporting Information Available: Graph showing the detrimental effect of chloride ions on the catalytic CV responses under PCR cycling conditions and experimental details and plots of the electrochemical real-time PCR experiments performed with the $Ru(bpy)_3^{2+}$/dGTP couple. This information is available free of charge via the Internet at http://pubs.acs.org.

JA901368M